Vector Field Aided Trajectory Tracking of a 10-gram Flapping-Wings Aerial Vehicle

Abdoullah Ndoye, José de Jesus Castillo-Zamora, Sabrine Samorah Laki, Romain Miot, Edwin van Ruymbeke, Franck Ruffier

Vector Field Aided Trajectory Tracking of a 10-gram Flapping-Wings Aerial Vehicle

A. Ndoye[1,*], J. J. Castillo-Zamora[1], S. Samorah-Laki[1], R. Miot[2], E. Van Ruymbeke [2] and F. Ruffier[1]

***Abstract*— In this paper, a 10-gram Flapping-Wings Aerial Vehicle (FWAV) is demonstrated to perform the automatic trajectory tracking task based on a vector fields method. In this regard, the reference for the heading control is provided by a vector field which is computed according to the desired trajectory. The FWAV is endowed with a directional mechanism which permits to exert the directional control command simultaneously by tensing one wing and relaxing the opposite wing and by moving the rudder in the same direction. Due to the complex phenomena involved in the dynamics, a set of dedicated free flight tests was performed to identify a simplified linear model using system identification in order to adjust the yaw controller and the roll inner loop controller avoiding stall. Our experimental results proved that our time-independent vector field-based strategy enlarges the initial conditions spectra in which stability is observed over tens of meters. The tracking of circular and 8-shaped trajectories was successfully accomplished.**

I. Introduction

During the last decade, Flapping-Wings Aerial Vehicles (FWAVs), also called ornithopters, have been increasingly drawing the attention of researchers who have devoted their effort to improve their agility [1–4] and control height [5,6] enhancing thus the FWAVs performance. Nowadays, FWAVs execute tasks such as obstacle avoidance [7–9], fixed-object tracking [10] and trajectory tracking [11–13].

In parallel, remote-controlled two-wing ornithopters weighing 10 grams have been commercialized since 2010 [14,15] and sold as crash-resistant toys by the company XTIM-BionicBird [i]. The successive versions of their RC models have been named Avitron, BionicBird, and lately Metafly: they are based on the same propulsion and directional mechanisms.

The Metafly (shown in Fig. 1) is endowed with 2 DC motors that serve as its actuators: one DC motor is attached to a 2-stage planetary gearbox to adjust the flapping frequency [14] meanwhile, the second DC motor concomitantly tenses one wing and relaxes the opposite wing (in a differential manner) while controlling the rudder to change the course [15]. Yet, the Metafly speed is poorly controllable as its flapping rate acts on both altitude and speed.

Regarding the agility of the FWAVs, it has been suggested that relying solely on a rudder to change the FWAVs direction may be inefficient as it does not generate the required force to permit agile maneuvers, even by using bang-bang control [16]. A commonly adopted solution is the so-called banked turn in which the roll motion is used to generate a change of direction [3,17] by means of wings dihedral [18,19], asymmetrical morphing of the wing surface [4], differential wings spoilers steering [20], or the generation of an asymmetric flapping amplitude [2,3,21], among others.

Fig. 1. The 10-gram Metafly Flapping-Wings Aerial Vehicle in Marseille's flight arena © Cyril Frésillon / ISM / CNRS Photothèque

Besides, the dynamics and kinematics of the FWAVs are complex such that a significant number of different dynamic models can be found in the literature [6,22–24]. Due to this complexity, most studies use fixed-wings models, ignoring the intra-flapping phenomena [25] and the actuators dynamics [3,26]. In these cases, grey-box [27,28] or black-box [12,29] systems identification results are suitable options to model the FWAVs dynamics.

Kim et al. [11,30] have succeeded to fly in formation 4 ornithopters along a circular trajectory. The cohesion of this formation was highly dependent on specific initial conditions and on the fine tuning of these ornithopters, as the authors themselves noticed [11].

As vector field-based trajectory tracking is time-independent [31–36], such strategy mitigate the poor controllability of the Metafly flight speed in order to track various trajectories, as shown in this paper. Our approach allows the vehicle (i) to robustly track the trajectory despite the initial conditions, (ii) to follow complex trajectories, and (iii) to change its trajectory in flight. The main contribution of our research is articulated about four axes:

- The role of adverse yaw in directional control.
- The identification of the simplified lateral linear model of the Metafly by means of real free flight data.
- A novel 3-state directional command (full left, neutral

[1] Aix Marseille Université, CNRS, ISM, Marseille, France
[2] XTIM - Bionic Bird, 13015 Marseille, France
[*] Corresponding author: abdoullah.ndoye@univ-amu.fr
[i] www.bionicbird.com

and full right) that permits to perform the directional control by tensing and relaxing the wings while positioning properly the rudder: the time the rudder remains full left or right serves as the control input.
- The first implementation of a vector field method on a FWAV (as far as we know) to time-independently track a trajectory and to enlarge the initial conditions range.

The outline of the paper is structured as follows: In Section II, the modified Metafly FWAV and its heading actuation are presented in detail. The system identification procedure, which was performed using real flight data and Matlab processing tools, is described, alongside the simplified model, in Section III. The vector field strategy implemented to track successfully various trajectories is given in Section IV. Section V show the results of different experimental tests that validate our vector field-based trajectory tracking proposal. Lastly, the concluding remarks and the future work are provided in Section VI.

II. The Metafly FWAV and its Heading Actuation

We used a modified version of the Metafly FWAV that embeds a Deltang RX43d receiver to control the two actuators, which adjusts the flapping frequency and actuates the directional mechanism, respectively. A 3.7V 58 mAh Lipo battery is used as power source. A list of the Metafly's characteristics is provided in Table I.

The heading actuation mechanism (described in Fig. 3) allows to change the heading by initiating a banked turn (as depicted in Fig.2). For example, to perform a left banked turn as in Fig.2, heading actuation mechanism tenses the right wing and relaxes the left wing while positioning the rudder left. It creates a negative rolling motion that induces a positive yawing moment. At the same time, there is also an important drag difference between the left and the right wing (due to the tensed right wing and the relaxed left wing) , leading also to a positive yawing moment in the same direction as the turn called here proverse yaw (Fig.2). During the rolling motion, as the left wing moves down, it hits an additional wind from below (see insert in Fig.2) that adds up with the velocity induced wind to give the resultant wind (grey arrows in Fig.2) oriented upward . The resulting opposite deflection of the lift (backward and forward) creates a negative yawing moment called adverse yaw (see red arrows in Fig.2). Adverse yaw only occurs during rolling.

The rudder also creates a small amount of positive yawing moment at the same direction as the induced yaw from the rolling motion and the proverse yaw to turn correctly making the effect of adverse yaw negligible.

TABLE I
METAFLY PARAMETERS AND PROPERTIES

Parameter/Property	Nominal value
Mass	10 [g]
Length	190 [mm]
Wingspan	290 [mm]
Wing chord	85 [mm]
Wing amplitude	$\pm 55°$
Flapping frequency	$10-20$ [Hz]
Flight endurance	8 [min]

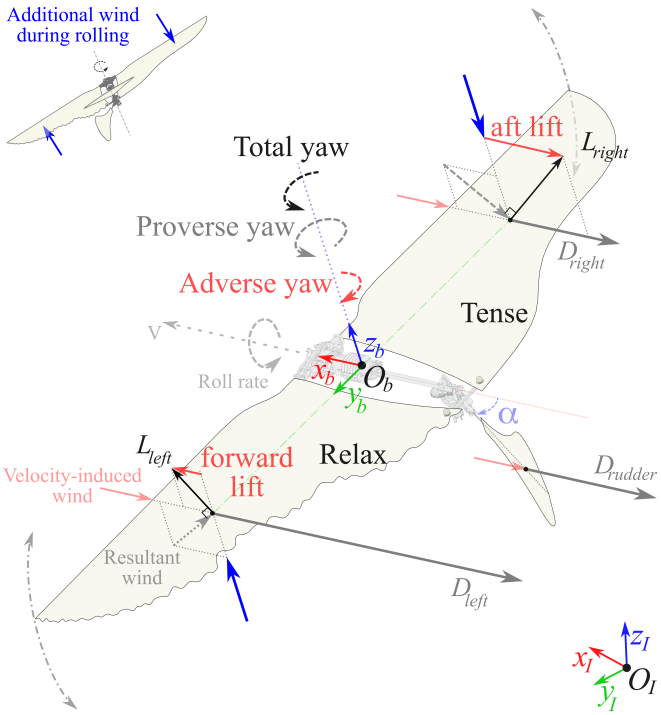

Fig. 2. On the Metafly, the directional mechanism concomitantly relaxes one wing (here, the left wing), tenses the opposite (here, the right wing), and turns the rudder (here to the left): it causes, in this case, a negative roll motion creating an induced positive yaw. Compared to the tensed right wing, the relaxed left wing produces a greater drag which causes a positive yaw moment (in the same turning direction): the proverse yaw. The additional wind (see insert) generated due to the roll motion causes a deflection of the lift vector. Adverse yaw appears as a direct consequence. The rudder (vertical tail) creates a small positive yaw moment that renders the Metafly more agile.

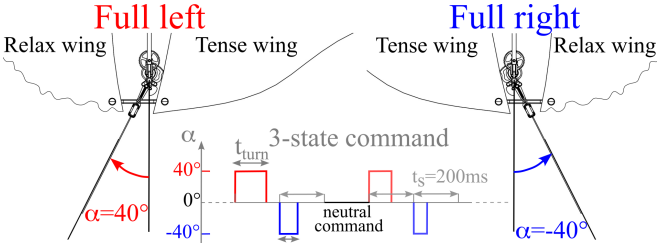

Fig. 3. The heading actuation system is a mechanism composed by a DC motor actuator that concomitantly turns the rudder and apply, at the same time, a differential tension on the wings (relax or tense), rendering more agility to the vehicle. A 3-state turning command (full-left, neutral and full-right) was used to apply efficiently the periodic command computed off-board. The periodic command $50 \geq t_{turn} \geq 150$ [ms] (at 5Hz) gives the duration of the pulse applied by the DC actuator to position the rudder at the maximum angle ($\alpha = \pm 40\,\text{deg}$) .

III. Metafly Modeling for the Heading Control

The identification of the Metafly dynamics between the directional command and the yaw (heading) was performed. As previously mentioned, the Metafly shall experience a roll motion to change its heading. If the roll angle Φ exceeds 35°, the Metafly will suffer a stall and start to descend rapidly.

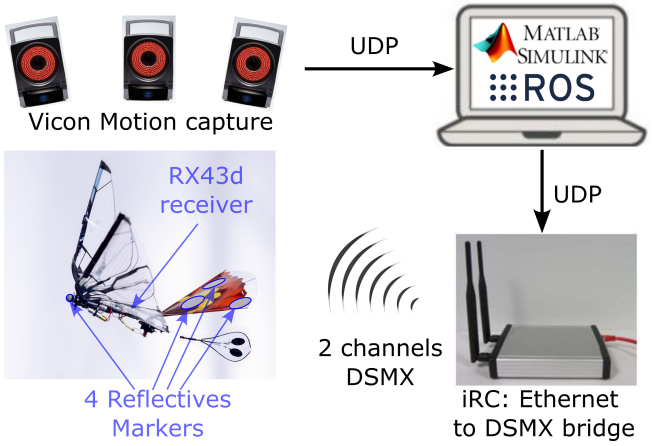

Fig. 4. Four reflective markers enabled the Metafly to be tracked by the Vicon motion capture system. The embedded RX43D receiver applies the computed commands of both, the flapping and the turn mechanisms, in real time.

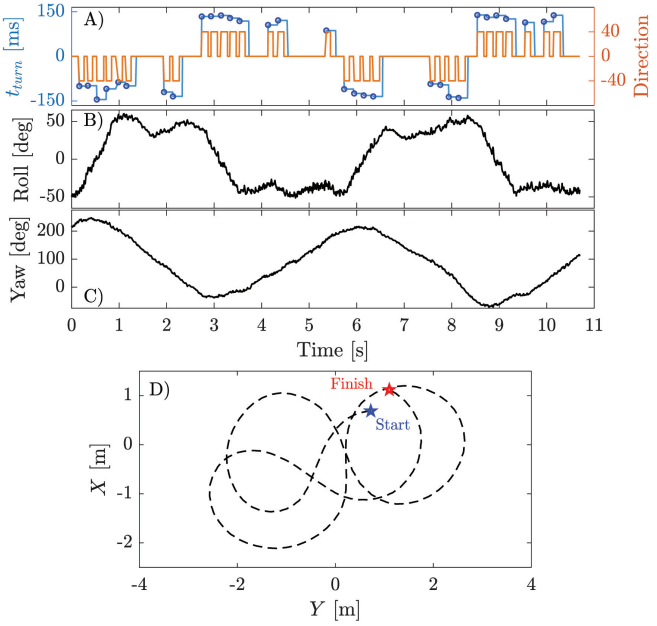

Fig. 5. During manual flight tests for identification, a small randomized signal is added to the signal generated by the joystick to enrich the data set before the identification process of $H_{roll/t_{turn}}$ and $H_{yaw/t_{roll}}$: A) Directional control input translated to the time-based control input t_{turn}. B) Roll due to the control input t_{turn}. C) Yaw during several banked turns. D) 2D trajectory of the Metafly during the flight test.

To mitigate this problem, roll motion shall be controlled and capped in an inner loop. Two transfer functions were identified: (i) $H_{roll/t_{turn}}(s)$ which relates the roll $\Phi(s)$ to the control input $t_{turn}(s)$, and (ii) $H_{yaw/roll}(s)$ that establishes the relation between the yaw $\Psi(s)$ and the roll $\Phi(s)$, such that:

$$H_{roll/t_{turn}}(s) = \frac{\phi(s)}{t_{turn}(s)} \quad \text{and} \quad H_{yaw/roll}(s) = \frac{\psi(s)}{\phi(s)} \tag{1}$$

A. Experimental Setup and Flight Tests

The identification experiments took place inside the flight arena. The effective volume, in which the 10-gram Metafly can be tracked at 500Hz by the Vicon motion capture system (17 cameras), was 90 [m^3] ($5\times6\times3$ [m] (lxLxH)). For these ends, a set of adhesive and spherical reflective markers was properly placed over the Metafly. The Metafly control is performed by an external workstation that runs Matlab and ROS, and sends the 2.4 Ghz DSMX signals to the RX43D receiver embedded on the Metafly (through an Ethernet to DSMX bridge, see Fig. 4).

Several free flight tests were performed to identify the black box model. In these experiments, the PID controller:

$$C_z(s) = k_d s + k_p + \frac{k_i}{s} = 1000s + 200 + \frac{0.1}{s} \tag{2}$$

was previously implemented such that the Metafly held its altitude constant w.r.t the ground by adapting its flapping frequency.

The latter led us to consider the flapping frequency as the only control input to stabilize the altitude of the Metafly and to use the rudder as the only actuation for the rotational motion. Nonetheless, as it was not possible to manipulate the rudder angle α all along the predefined range, we adopted the 3-state turning command strategy, exposed in Fig 3, considering thus the time t_{turn} as the actual rotational control input. Notice that the position of the rudder, (full left, neutral, full right) is defined by the sign of t_{turn} such that a negative value is referred to the full right position, and a positive value stands for full left position. The zero command is related to $\alpha = 0°$ (see Fig. 3). As shown in Fig. 5, the data concerning t_{turn}, Φ and Ψ are recorded to implement the Matlab System Identification Toolbox.

B. Model Identification

According to the data recorded during 4 different free flight tests, the functions $H_{roll/t_{turn}}(s)$ and $H_{yaw/roll}(s)$ were identified, by the Gauss-Newton search method, as:

$$H_{roll/t_{turn}}(s) = -\frac{0.4536s + 0.09858}{s^2 + 0.7815s + 0.1387} \tag{3}$$

$$H_{yaw/roll}(s) = -\frac{7.455s + 8.179}{s^2 + 1.493s + 0.01036} \tag{4}$$

The data from one of the tests were selected to be used for identification purposes. The reminder of the data was used during the validation stage. In this regard, with a given fit percentage of 78% and 86% for $H_{roll/t_{turn}}(s)$ and $H_{yaw/roll}(s)$, respectively, we considered that the transfer functions had been successfully identified. Both identified transfer function were used in simulation for controllers tuning presented in the next section.

IV. Vector Field-Based Trajectory Tracking

A. The Vector Field theory

A vector field assigns a vector to each point of plane with a direction allowing to converge to a desired path [33]. Let us consider the position of the robot in the corresponding horizontal plane, $\xi = [x\ y]^T \in \mathbb{R}^2$ and recall the orientation of the robot as $\Psi_{meas} \in \mathbb{R}$ [33], such that its velocity can be

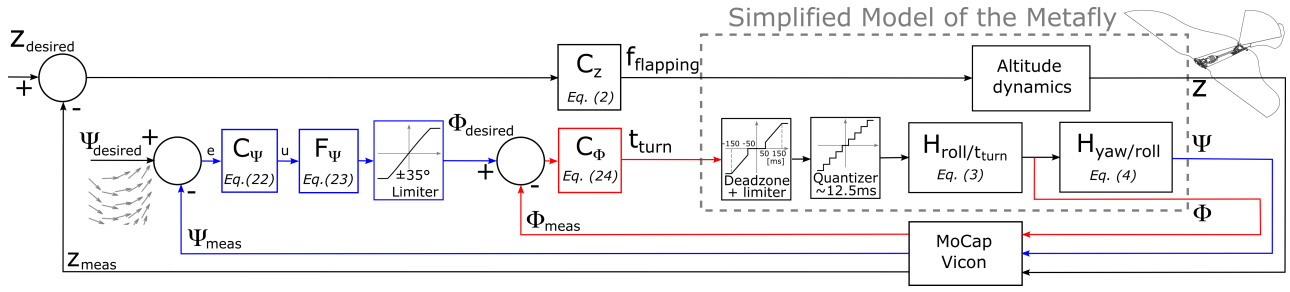

Fig. 6. Control scheme of the Metafly, including the heading model. Two non-linearities (a deadzone/limiter and a quantizer) and two transfer functions, the heading dynamics (roll and yaw, respectively). The deadzone models the minimum time the DC motor should actuate the heading actuation system. The quantizer models, approximately, the HF refresh rate. The inner loop maintains the roll between ± 35 deg to prevent stall. The heading outer loop controls the yaw according to the vector field $\Psi_{desired}$ while the altitude control loop maintains the height constant.

written as

$$\dot{\xi} = v_{flight} \begin{bmatrix} \cos(\Psi_{meas}) \\ \sin(\Psi_{meas}) \end{bmatrix} = v\chi_u \in \mathbb{R}^2 \tag{5}$$

where $v_{flight} \in \mathbb{R}$ is the flight speed (for instance, considered as constant since the flapping frequency is fixed by the altitude controller) and $\chi_u \in \mathbb{R}^2$ is the directional unit vector. Additionally, one can define a curvilinear desired path by the implicit equation:

$$\mathscr{P} = \{\xi_d : \varphi(\xi_d) = 0\} \subset \mathbb{R}^2 \tag{6}$$

such that the function $\varphi : \mathbb{R} \to \mathbb{R}^2$ is C^2-smooth. The geometric curve $\mathscr{P}$ can be represented in several implicit forms. The principal restriction imposed to the curvilinear path is regularity, i.e. in some vicinity of $\mathscr{P}$ one has:

$$\|\nabla\varphi(\xi_d)\| = \left\| \begin{bmatrix} \frac{\partial\varphi(\xi_d)}{\partial x_d} & \frac{\partial\varphi(\xi_d)}{\partial y_d} \end{bmatrix}^T \right\| \neq 0 \tag{7}$$

where $\|\bullet\|$ stands for the euclidean norm.
The tracking error e_{track} is defined by a strictly increasing C^1-function $\varepsilon(\bullet)$ such that:

$$e_{track}(\xi) = \varepsilon[\varphi(\xi)] \in \mathbb{R} \tag{8}$$

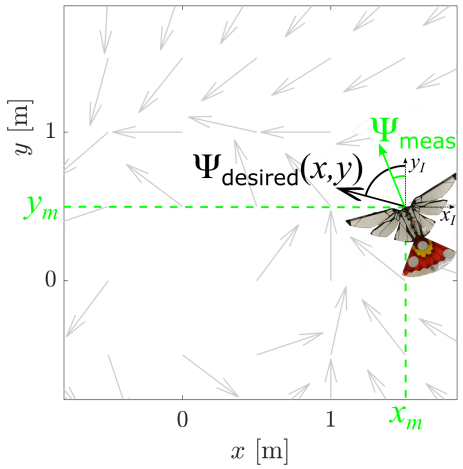

Fig. 7. Vector field clockwise converging to a circle of radius 1 and centered at (0,0). Desired orientation $\Psi_{desired}$ and the actual heading of the Metafly measured by the Vicon system (Ψ_{meas}).

The selection of $\varepsilon(\bullet)$ is a free parameter. By definition $e_{track} = 0$ if and only if $\xi \in \mathscr{P}$. Thus, according to [37], the vector field χ can be constructed by the expression:

$$\chi(\xi_d) = (\Gamma - k_n e_{track}(\xi_d) I_2) \nabla\varphi(\xi_d) \tag{9}$$

with $k_n = \text{const} > 0$,

$$\Gamma = \begin{bmatrix} 0 & \gamma \\ -\gamma & 0 \end{bmatrix} \in \mathbb{R}^{2\times 2} \quad \text{and} \quad I_2 = \begin{bmatrix} 1 & 0 \\ 0 & 1 \end{bmatrix} \in \mathbb{R}^{2\times 2} \tag{10}$$

Notice that $\gamma \in \{-1, 1\}$ determines in which direction $\mathscr{P}$ will be tracked. Thus Eq. (9) is used to find the desired directional unit vector field χ_{u_d} and, as consequence, $\Psi_{desired}$ as follows:

$$\chi_{u_d} = \frac{\chi(\xi_d)}{\|\chi(\xi_d)\|} = \begin{bmatrix} \chi_{x_d} \\ \chi_{y_d} \end{bmatrix} \tag{11}$$

$$\Psi_{desired} = \text{atan2}(\chi_{y_d}, \chi_{x_d}) \tag{12}$$

In addition, the derivative of χ_{u_d} along its trajectories, $\dot{\chi}_{u_d}$, is provided by:

$$\dot{\chi}_{u_d} = -\omega_d \Gamma \chi_{u_d} = \begin{bmatrix} \dot{\chi}_{x_d} \\ \dot{\chi}_{y_d} \end{bmatrix} \tag{13}$$

$$\tag{14}$$

Considering that $\left\|\chi_{u_d}\right\| = 1$ and $\chi_{u_d}^T \dot{\chi}_{u_d} = 0$, ω_d is a scalar function that can be explicitly found from the set of equations:

$$\begin{cases} \dot{\chi}(\xi_d) = (\Gamma - k_n e_{track}(\xi_d) I_2) H(\xi_d) \dot{\xi}_d - k_n \dot{e}_{track}(\xi_d) \nabla\varphi(\xi_d) \\ \dot{e}_{track}(\xi_d) = \varepsilon'(\varphi(\xi_d)) [\nabla\varphi(\xi_d)]^T \dot{\xi}_d \\ \dot{\chi}_{u_d} = \frac{d}{dt} \frac{\chi(\xi_d)}{\|\chi(\xi_d)\|} = -\frac{1}{\|\chi(\xi_d)\|} \Gamma \chi_{u_d} \chi_{u_d}^T \Gamma \dot{\chi}(\xi_d) \end{cases} \tag{15}$$

where $H(\xi_d)$ stands for the Hessian:

$$H(\xi_d) = \begin{bmatrix} \frac{\partial^2}{\partial x_d^2}\varphi(\xi_d) & \frac{\partial^2}{\partial x_d \partial y_d}\varphi(\xi_d) \\ \frac{\partial^2}{\partial y_d \partial x_d}\varphi(\xi_d) & \frac{\partial^2}{\partial y_d^2}\varphi(\xi_d) \end{bmatrix} \tag{16}$$

For instance, let us recall the implicit function that describes a circle of radius $r > 0$ and centered at $c = [c_x \; c_y]^T \in \mathbb{R}^2$, defining thus $\varphi(\xi_d)$ as:

$$\varphi(\xi_d) = (x_d - c_x)^2 + (y_d - c_y)^2 - r^2 \tag{17}$$

Considering $e_{track}(\xi) = \varphi(\xi)$, $\gamma = -1$ and $k_n = 1$, Eq. (9) applied over Eq. (17) gives the vector field:

$$\chi(\xi_d) = 2\begin{bmatrix} -\varphi(\xi_d) & -1 \\ 1 & -\varphi(\xi_d) \end{bmatrix}\begin{bmatrix} x_d - c_x \\ y_d - c_y \end{bmatrix} \tag{18}$$

From where the directional unit vector field and its derivative, χ_{u_d} and $\dot{\chi}_{u_d}$, are computed. Fig.7 shows the directional unit vector field of a circle with $r = 1$ and $c = [0\ 0]^T$ which was used to perform the experimental tests and whose vector field is described by the expression:

$$\chi_0(\xi_d) = \begin{bmatrix} -x^3 - xy^2 + x - y \\ -y^3 - x^2 y + x + y \end{bmatrix} \tag{19}$$

B. Roll and Yaw controllers

Once the desired attitude is set, based on the vector field (Eq. 18), the heading error and its derivative can be written as:

$$e = \Psi_{desired} - \Psi_{meas} = \text{atan2}\left(\chi_{y_d}, \chi_{x_d}\right) - \Psi_{meas} \tag{20}$$

$$\dot{e} = \frac{\chi_{y_d}\dot{\chi}_{x_d} - \dot{\chi}_{y_d}\chi_{x_d}}{\chi_{y_d}^2 + \chi_{x_d}^2} - \dot{\Psi}_{meas} \tag{21}$$

The latter permits us to define a modified PD controller of the form:

$$u = \text{sawtooth}(e) + \dot{e} \tag{22}$$

which gives a reference value that is passed through filter $F_\Psi(s)$ to compute the roll reference $\Phi_{desired}$. The function sawtooth$(\bullet)$ serves as a wrapping function to fit the yaw angle between 0 and 360 [deg].

To carry out the experimentation, the control scheme depicted in Fig. 6 was followed. In this regard, a constant setpoint $Z_{desired}$ was given to the vehicle in order to keep its altitude constant by updating the flapping frequency command according to the action of the PID controller $C_z(s)$ and the information provided by the MoCap Vicon i.e. the position and the orientation. The directional closed loop control considers the desired yaw angle $\Psi_{desired}$ computed with the vector field. Once this reference value has been computed, it is compared to the actual yaw angle Ψ_{meas} of the Metafly such that the PD controller C_Ψ and the filter F_Ψ produce the appropriate desired roll angle that is limited between $-35°$ and $35°$ to prevent stall, afterwards, it is contrasted with the actual roll angle. The resulting error is thus treated by the lead controller C_Φ that sends the t_{turn} command to action the rudder. The attitude of the Metafly is equally tracked by the MoCap Vicon.

The lead controller C_Φ and the filter F_Ψ were set in simulation that included all non-linearities (fig. 6) as well as the identified transfer functions ($H_{roll/t_{turn}}$ and $H_{yaw/roll}$) presented in section III. These controllers were tuned until considering an acceptable behavior in automated flight. The filter F_Ψ, and the lead controller C_Φ respectively for roll and yaw control, were defined as:

$$F_\Psi(s) = 1.28\left(\frac{s+0.1}{s+0.3}\right)\left(\frac{s+0.1}{s+0.3}\right) \tag{23}$$

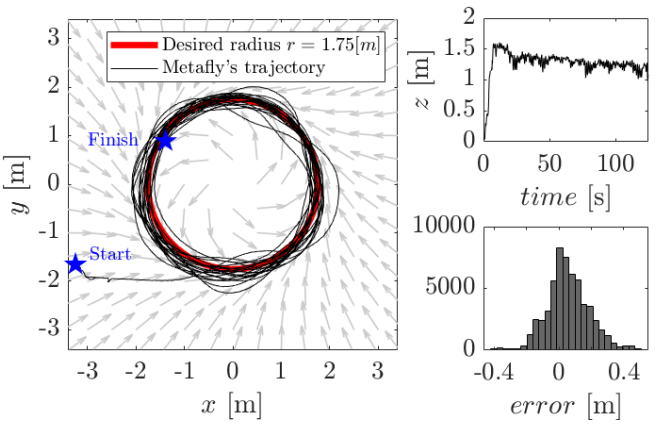

Fig. 8. Results of a circular trajectory tracking test by means of the vector field approach: The circle of radius 1.75m was centered at the origin. Average flight altitude $z = 1.3$m. 21 turns completed.

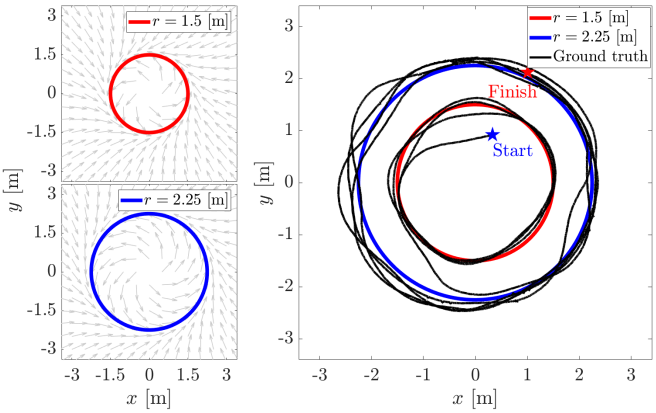

Fig. 9. Metafly FWAV tracking an in-flight modified circular trajectory: the vehicle followed, during 4 turns, a circular trajectory with a radius of 1.5m before following, for another 4 turns, a circular trajectory of radius 2.25m.

$$C_\Phi(s) = 3\left(\frac{s+0.015}{s+0.055}\right)\left(\frac{s+0.015}{s+0.0553}\right) \tag{24}$$

The controllers were used for the automated trajectory tracking presented in the next section.

V. Experimental Results

Using the vector fields, and the 3-state directional command, we demonstrated successful circular trajectory tracking of the Metafly based on the model described in section III and the controllers that were found. In Fig. 8, the Metafly successfully completed 21 tours of a circle of radius 1.75m (around 230m) while maintaining its altitude. The error distribution is centered at 0.0548m and its standard deviation is 0.128m. Table. II summarize the performances achieved for circular trajectory tracking with the mean error on the radius close to 0.

In Fig. 9, the Metafly is able to change the radius during its circular trajectory : it performed 4 laps of a circle of radius 1.5m before changing its trajectory to perform 4 laps of a circle of radius 2.25m.

Using the vector fields method, the Metafly is also able to follow complex trajectories: an 8-shaped circuit for example

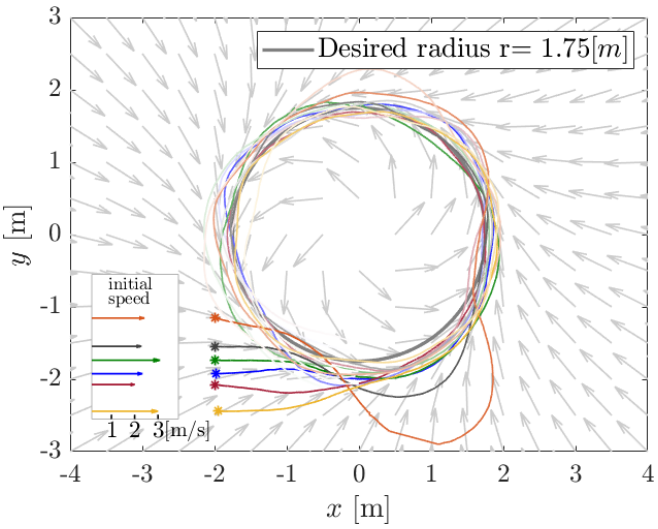

Fig. 10. Trajectory tracking of a circular path of radius 1.5 [m] under different initial velocity conditions: initial velocity profile between 1.9 and 3.14 [m/s].

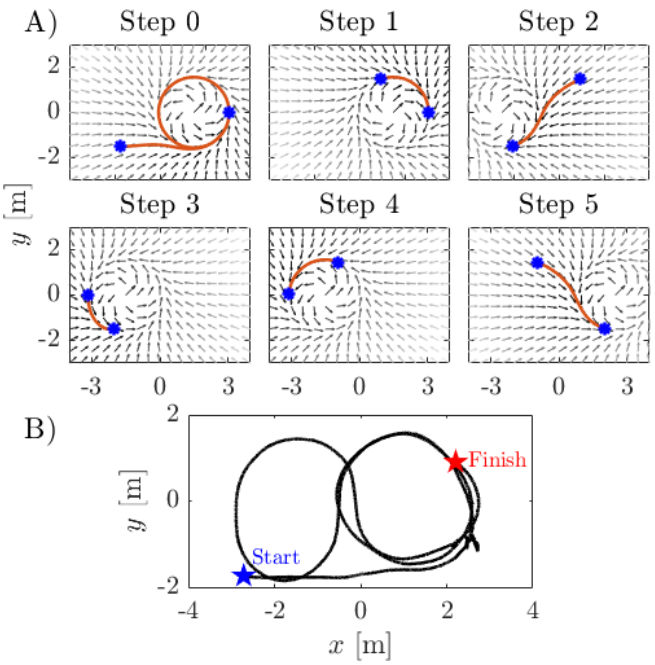

Fig. 11. Metafly FWAV tracking an 8-shape trajectory: A) Steps segmentation according to the position of the vehicle to create an 8-shape circuit with vector fields. B) Resulting 8-shape trajectory performed by the Metafly.

is built using different steps, each step being a section of the 8-shaped trajectory obtained with a vector fields converging to a circle (Fig. 11).

The use of vector fields method for flapping-wings MAV is one of the main contribution of this paper. As discussed in the introduction, the vector fields allow to track a trajectory despite non-strict initial conditions in position and speed.

In Fig. 10, different tests were performed with different initials conditions. The circular trajectory tracking was successfully completed with initial speed from 2m/s to 3m/s and various positions along a 1.25m-wide start line.

TABLE II

PERFORMANCES DURING CIRCULAR TRAJECTORY TRACKING IN FIG. 8

	std [m]	**mean [m]**	**median [m]**
Radius error	0.128	0.0548	0.0459
Altitude error	0.1040	0.2	0.2078

VI. CONCLUSION

In this paper, we demonstrated successful trajectory tracking of a 10-gram FWAV, the Metafly using vector field method for the first time (to the best of our knowledge). Vector field method is proven to be time-independent and allows the Metafly to track trajectories a various range of initial condition in terms of position and velocity. Our results showed that black box system identification based on enriched manual flight test data can be effective for controller design purpose of FWAV. The proposed 3-state directional command allowed the Metafly to perform trajectory tracking of a circle and of an 8-shaped circuit maintaining constant altitude. In future works, it could be interesting to embed sensors, such as micro-GPS, gyro, magnetometer, or optic flow sensors, to perform vector field-based trajectory tracking in presence of wind and obstacles, outdoors.

ACKNOWLEDGMENT

We thank J.M. Ingargiola for the electronics, J. Diperi for the micro-mechanics, C. Coquet for the Vicon system, A. Negre & J. Dumond for the HF connection and S. Durand for proofreading. Financial support was provided by a RAPID Biofly grant to E.V.R. & F.R. from the AID/DGA.

REFERENCES

[1] M. Keennon, K. Klingebiel, and H. Won, "Development of the nano hummingbird: A tailless flapping wing micro air vehicle," in *50th AIAA aerospace sciences meeting including the new horizons forum and aerospace exposition*, 2012, p. 588.

[2] K. Y. Ma, P. Chirarattananon, S. B. Fuller, and R. J. Wood, "Controlled flight of a biologically inspired, insect-scale robot," *Science*, vol. 340, no. 6132, pp. 603–607, 2013.

[3] M. Karásek, F. T. Muijres, C. De Wagter, B. D. Remes, and G. C. De Croon, "A tailless aerial robotic flapper reveals that flies use torque coupling in rapid banked turns," *Science*, vol. 361, no. 6407, pp. 1089–1094, 2018.

[4] A. Chen, B. Song, Z. Wang, D. Xue, and K. Liu, "A novel actuation strategy for an agile bioinspired fwav performing a morphing-coupled wingbeat pattern," *IEEE Transactions on Robotics*, 2022.

[5] S. S. Baek and R. S. Fearing, "Flight forces and altitude regulation of 12 gram i-bird," in *2010 3rd IEEE RAS & EMBS International Conference on Biomedical Robotics and Biomechatronics*. IEEE, 2010, pp. 454–460.

[6] W. He, H. Huang, Y. Chen, W. Xie, F. Feng, Y. Kang, and C. Sun, "Development of an autonomous flapping-wing aerial vehicle," *Science China Information Sciences*, vol. 60, no. 6, pp. 1–8, 2017.

[7] G. C. De Croon, M. Groen, C. De Wagter, B. Remes, R. Ruijsink, and B. W. van Oudheusden, "Design, aerodynamics and autonomy of the delfly," *Bioinspiration & biomimetics*, vol. 7, no. 2, p. 025003, 2012.

[8] C. De Wagter, S. Tijmons, B. D. W. Remes, and G. C. H. E. de Croon, "Autonomous flight of a 20-gram flapping wing mav with a 4-gram onboard stereo vision system," in *2014 IEEE International Conference on Robotics and Automation (ICRA)*, 2014, pp. 4982–4987.

[9] S. Tijmons, C. De Wagter, B. Remes, and G. De Croon, "Autonomous door and corridor traversal with a 20-gram flapping wing mav by onboard stereo vision," *Aerospace*, vol. 5, no. 3, p. 69, 2018.

[10] S. S. Baek, F. L. G. Bermudez, and R. S. Fearing, "Flight control for target seeking by 13 gram ornithopter," in *2011 IEEE/RSJ International Conference on Intelligent Robots and Systems*. IEEE, 2011, pp. 2674–2681.

[11] H.-Y. Kim, J.-S. Lee, H.-L. Choi, and J.-H. Han, "Autonomous formation flight of multiple flapping-wing flying vehicles using motion capture system," *Aerospace Science and Technology*, vol. 39, pp. 596–604, 2014.

[12] J. Oh, S. Kim, B. Lee, S. Kim, and J. Suk, "System identification & attitude control of avian-type flyer with flight test," in *2017 11th Asian Control Conference (ASCC)*. IEEE, 2017, pp. 1677–1682.

[13] J. Hoff, U. Syed, A. Ramezani, and S. Hutchinson, "Trajectory planning for a bat-like flapping wing robot," in *2019 IEEE/RSJ International Conference on Intelligent Robots and Systems (IROS)*. IEEE, 2019, pp. 6800–6805.

[14] E. Van Ruymbeke, D. Van Ruymbeke, Y. Van Ruymbeke-Caranoni, and G. Van Ruymbeke, "Flying toy able to move by the flapping of wings," Feb. 11 2010, PCT, WO2010015781A1.

[15] E. Van Ruymbeke, "Flying toy able to move by the flapping of wings," Feb. 26 2013, US Patent 8,382,546.

[16] S. Ryu, U. Kwon, and H. J. Kim, "Autonomous flight and vision-based target tracking for a flapping-wing mav," in *2016 IEEE/RSJ International Conference on Intelligent Robots and Systems (IROS)*. IEEE, 2016, pp. 5645–5650.

[17] F. Ruffier, "Robotic-flapper maneuvers and fruitfly turns," *science*, vol. 361, no. 6407, pp. 1073–1074, 2018.

[18] P. Muren, "System for controlling flight direction," Dec. 25 2012, uS Patent 8,336,809.

[19] A. A. Paranjape, S.-J. Chung, and J. Kim, "Novel dihedral-based control of flapping-wing aircraft with application to perching," *IEEE Transactions on Robotics*, vol. 29, no. 5, pp. 1071–1084, 2013.

[20] G. A. Folkertsma, W. Straatman, N. Nijenhuis, C. H. Venner, and S. Stramigioli, "Robird: a robotic bird of prey," *IEEE robotics & automation magazine*, vol. 24, no. 3, pp. 22–29, 2017.

[21] M. Karasek, A. Hua, Y. Nan, M. Lalami, and A. Preumont, "Pitch and roll control mechanism for a hovering flapping wing mav," *International Journal of Micro Air Vehicles*, vol. 6, no. 4, pp. 253–264, 2014.

[22] J. D. DeLaurier, "An aerodynamic model for flapping-wing flight," *The Aeronautical Journal*, vol. 97, no. 964, pp. 125–130, 1993.

[23] A. Banazadeh and N. Taymourtash, "Adaptive attitude and position control of an insect-like flapping wing air vehicle," *Nonlinear Dynamics*, vol. 85, no. 1, pp. 47–66, 2016.

[24] A. Bakhtiari, S. Ehtemadi Haghighi, and A. Maghsoudpour, "Modeling and control of a flapping wing robot," *Proceedings of the Institution of Mechanical Engineers, Part K: Journal of Multi-body Dynamics*, vol. 233, no. 1, pp. 174–181, 2019.

[25] A. Ndoye, S. S. Laki, R. Miot, E. van Ruymbeke, and F. Ruffier, "Ornithopter's intra-flapping body pitch highly depends on wingbeat frequency," *Computer Methods in Biomechanics and Biomedical Engineering*, vol. 24, no. Sup 1, pp. S101–S103, 2021.

[26] W. He, X. Mu, L. Zhang, and Y. Zou, "Modeling and trajectory tracking control for flapping-wing micro aerial vehicles," *IEEE/CAA Journal of Automatica Sinica*, vol. 8, no. 1, pp. 148–156, 2020.

[27] J. Grauer, E. Ulrich, J. Hubbard Jr, D. Pines, and J. S. Humbert, "Testing and system identification of an ornithopter in longitudinal flight," *Journal of Aircraft*, vol. 48, no. 2, pp. 660–667, 2011.

[28] H. Gim, S. Kim, J. Suk, and S. Cho, "Longitudinal system identification of ornithopter with automated flight tests," *IFAC-PapersOnLine*, vol. 49, no. 17, pp. 194–199, 2016.

[29] S. F. Armanini, C. C. de Visser, and G. de Croon, "Black-box lti modelling of flapping-wing micro aerial vehicle dynamics," in *AIAA atmospheric flight mechanics conference*, 2015, p. 0234.

[30] H.-Y. Kim, J.-S. Lee, and J.-H. Han, "An indoor autonomous flight of multiple ornithopters following a circular path," in *2014 14th International Conference on Control, Automation and Systems (ICCAS 2014)*. IEEE, 2014, pp. 844–847.

[31] D. R. Nelson, D. B. Barber, T. W. McLain, and R. W. Beard, "Vector field path following for miniature air vehicles," *IEEE Transactions on Robotics*, vol. 23, no. 3, pp. 519–529, 2007.

[32] D. Zhou and M. Schwager, "Vector field following for quadrotors using differential flatness," in *2014 IEEE international conference on robotics and automation (ICRA)*. IEEE, 2014, pp. 6567–6572.

[33] L. Jaulin, *Mobile robotics*. John Wiley & Sons, 2019.

[34] J. P. Wilhelm and G. Clem, "Vector field uav guidance for path following and obstacle avoidance with minimal deviation," *Journal of Guidance, Control, and Dynamics*, vol. 42, no. 8, pp. 1848–1856, 2019.

[35] A. M. Rezende, V. M. Gonçalves, A. H. Nunes, and L. C. Pimenta, "Robust quadcopter control with artificial vector fields," in *2020 IEEE International Conference on Robotics and Automation (ICRA)*. IEEE, 2020, pp. 6381–6387.

[36] W. Yao, H. G. de Marina, Z. Sun, and M. Cao, "Distributed coordinated path following using guiding vector fields," in *2021 IEEE International Conference on Robotics and Automation (ICRA)*. IEEE, 2021, pp. 10 030–10 037.

[37] Y. A. Kapitanyuk, H. G. de Marina, A. V. Proskurnikov, and M. Cao, "Guiding vector field algorithm for a moving path following problem," *IFAC-PapersOnLine*, vol. 50, no. 1, pp. 6983–6988, 2017.